Steam reforming of sunflower oil over Ni/Al catalysts prepared from hydrotalcite-like materials

Maximiliano Marquevich, Xavier Farriol, Francisco Medina, and Daniel Montané *

Department of Chemical Engineering, ETSEQ, Rovira i Virgili University, Avinguda dels Països Catalans 26, 43007 Tarragona (Catalunya), Spain

Received 21 May 2002; accepted 19 September 2002

Using catalytic steam reforming of biofuels to produce hydrogen for energy systems based on fuel cells is an option that may help to reduce the net emissions of CO_2 into the atmosphere. Vegetable oils are some of the most interesting options because of their high potential yield of hydrogen. They are, however, more difficult to reform than the light hydrocarbon feedstocks that are used for producing hydrogen industrially by steam reforming. Catalysts prepared from hydrotalcite-like materials are promising for use in the steam reforming of vegetable oils, since their catalytic activity is significantly higher than that of commercial catalysts for hydrocarbon steam reforming. In this paper, a study is made of how the nickel content of HT-derived catalysts affects their activity for steam reforming of sunflower oil. Three catalysts were prepared with Ni/Al atomic ratios of 1, 2, and 3, respectively. The samples were characterized by various techniques to correlate their activity with the structural characteristics of the catalysts: X-ray diffraction (XRD), BET, thermogravimetric analysis (TGA), and hydrogen chemisorption. The results showed that the catalyst activity increased as the nickel content in the material decreased. The support and its properties seemed to play a key role in the performance of the HT-derived catalysts. This is probably because a decrease in the Ni content produces a better dispersion of the metal and higher BET areas, which leads to a higher capacity for water adsorption. With the most active catalyst (Ni/Al of 1), 2.2 mol $H_2/(g_{cat}\,h)$ was produced at 575 °C, 2 bar, and a steam-to-carbon ratio of 3.

KEY WORDS: steam reforming; vegetable oils; hydrotalcite-like materials; nickel catalysts; hydrogen production; biofuels.

1. Introduction

Using hydrogen as a fuel and energy carrier is one way of creating an energy system that has less impact on the environment, especially in terms of the emission of gases linked to the greenhouse effect [1,2]. One problem with this hypothetical hydrogen-based energy system is that the technology involved in the production of hydrogen today has a strong effect on the environment. Most hydrogen is produced on an industrial scale from natural gas, LPG, and naphtha by catalytic steam reforming, or from heavy oil fractions by partial oxidation [3]. Consequently, since hydrogen production is based on fossil fuels, it is a net contributor to carbon dioxide emissions and the greenhouse effect. For example, life-cycle inventory analysis of the production of hydrogen in a steam reforming plant based on natural gas with a capacity of $1.5 \times 10^6\,Nm^3$/day shows that the amount of fossil CO_2-equivalent released into the atmosphere is 1374.5 kg to produce 100 kg of hydrogen gas [4]. Clearly, unless hydrocarbon-based technology is upgraded to incorporate effective methods of carbon sequestration [5], other options are needed. For the near- and mid-term, generating hydrogen from renewable biomass may be the most practical and viable option [6]. The rationale behind this approach is the fact that the CO_2 released into the atmosphere when thermochemically converting biomass is offset by the uptake of CO_2 during biomass growth, thus providing a potentially carbon-neutral process. Although the contribution made by other gases to global warming (e.g. methane and nitrous oxide generated during biomass harvesting and processing) must be taken into account, this biomass-based scenario has potential as a sustainable process for producing hydrogen. There are two ways of thermochemically converting biomass to produce hydrogen: (i) gasification followed by water-shift [7–10], and (ii) steam reforming of biomass-derived liquids (biofuels), coupled with water-shift to approach the stoichiometric yield of hydrogen. Several biofuels have been studied: liquids from flash pyrolysis of lignocellulosics (i.e. bio-oil) [11–16], bioethanol [17–19], and vegetable oils [20–22]. We are currently focusing our research on vegetable oils because they are a promising feedstock for energy applications (bio-diesel) [23–25]. We believe that vegetable oils are an interesting feedstock for producing hydrogen because of their low oxygen content and subsequent high potential yields of hydrogen. Vegetable oils are formed by fatty acids of 16 to 20 carbon chains, which are more difficult to reform than natural gas, LPG, or naphtha, the usual hydrocarbon feedstocks for producing hydrogen by industrial steam reforming. Therefore, steam reforming catalysts must have good stability and high catalytic activity, and also be adapted to organic molecules of high molecular weight.

Nickel-based hydrotalcite-like (HT) materials have properties that make them suitable for preparing

* To whom correspondence should be addressed.
E-mail: dmontane@etseq.urv.es

1011-372X/03/0100-0041/0

promising steam reforming catalysts. HT materials that belong to the class of anionic clays have a brucite-like $Mg(OH)_2$ network in which an isomorphous substitution of Mg^{2+} by a trivalent element M^{3+} occurs. The structure of the hydrotalcite is very similar to that of brucite. In brucite, each magnesium cation is octahedrally surrounded by hydroxyls. The resulting octahedron shares edges to form infinite sheets with no net charge. When Mg^{2+} ions are replaced by a trivalent ion (which, like Al^{3+}, does not have too different a radius), a positive charge is generated in the brucite sheet. The positively charged Mg–Al double hydroxide sheets (or layers) are charge-balanced by the carbonate anions in the interlayer sections of the clay structure. In the free space of this interlayer, the water of crystallization also finds a place [26–30]. The HT compounds are generally described by the empirical formula $[(M^{2+})_n(M^{3+})_m(OH)_{2(n+m)}]^{m+}[(A^{x-})_{m/x}\cdot yH_2O]$, where M^{2+} and M^{3+} are metal cations, A represents the x-valent anion needed to compensate the net positive charge, x is the charge of the anion, the $m/(m+n)$ ratio may vary from 0.17 to 0.33 depending on the particular combination of di- and trivalent elements, and y is the number of interlayer water molecules. HT compounds easily decompose into a mixed oxide of the $M^{2+}M^{3+}(O)$ type upon calcination. Further reduction of HT compounds, or mixed oxides containing reducible cations, yields supported metal catalysts. In these materials the metallic function and the acid–base properties can be tailored through such parameters as the nature and number of the cations in the layers and the activation conditions [31]. This class of supported metal catalysts has been reported to have properties that are similar to those of hydrogenation and steam reforming catalysts [30,33–39]. We recently observed that, when steam reforming sunflower oil, catalysts prepared from hydrotalcite-like materials are approximately ten times more active than commercial steam reforming catalysts designed for hydrocarbon steam reforming [21,22].

In this paper we report on the catalytic properties of hydrotalcite-like precursors with different Ni^{2+}/Al^{3+} atomic ratios for the production of hydrogen from sunflower oil. The process conditions are similar to those of steam reforming naphtha. We conducted a systematic study to determine how the reforming temperature, the steam-to-carbon ratio, and, more specifically, the amount of nickel in the catalyst affected the activity of the material. The samples were characterized by different techniques in order to correlate the activity with the structural characteristics of the catalysts.

2. Experimental

2.1. Catalyst preparation

Three hydrotalcite-like materials with nominal Ni^{2+}/Al^{3+} atomic ratios of 1, 2, and 3 were prepared and labeled, respectively, as HT_1, HT_2, and HT_3. They were obtained by co-precipitation at room temperature from two aqueous solutions at constant $pH = 9.0 \pm 0.2$. One solution contained appropriate amounts of $Ni(NO_3)_2\cdot 6H_2O$ and $Al(NO_3)_3\cdot 9H_2O$, and the other was an aqueous solution of NaOH (1 M) and $NaHCO_3$ (1 M). The solutions were mixed in a glass reaction vessel (500 cm^3) initially containing 100 mL of deionized water. The addition was performed drop by drop under vigorous magnetic stirring. After complete precipitation, the gel was treated for 2 h at 80 °C. Then the gel was recovered by filtration and washed several times with distilled water. The solid was then dried in an oven at 100 °C for 72 h. The Ni/Al content in the co-precipitate was determined by EDAX (energy dispersive analysis using X-rays) and atomic absorption spectroscopy. The results obtained from both techniques were in good agreement and are given in table 1. A sample of the solid was heated at 1 °C/min in air to 400 °C, and was calcinated at this temperature for 4 h. The calcinated solid was pelletized and reduced at 600 °C in a nitrogen stream with 20% of hydrogen to obtain Cat_1, Cat_2, and Cat_3 from HT_1, HT_2, and HT_3, respectively. The degree of reduction of the sample was determined from the consumption of hydrogen.

2.2. BET area

BET surface areas were calculated from the nitrogen adsorption isotherms at 77 K using a Micromeritics ASAP 2000 surface analyzer, and a value of 0.164 nm^2 for the cross-section of the nitrogen molecule.

2.3. Hydrogen chemisorption

The hydrogen chemisorption was measured with a Micromeritics ASAP 2010C instrument equipped with

Table 1
Chemical composition of the hydrotalcite-like precursors

Compound	Formula	Composition after calcination at 400 °C (wt%)
HT_1	$Ni_{0.98}Al_1(OH)_{3.96}(NO_3)_{0.08}(CO_3)_{0.67}\times 2.7\ H_2O$	46.7 Ni, 21.5 Al, 31.8 O
HT_2	$Ni_{2.01}Al_1(OH)_{6.02}(NO_3)_{0.04}(CO_3)_{0.48}\times 2.5\ H_2O$	58.6 Ni, 13.5 Al, 27.9 O
HT_3	$Ni_{2.82}Al_1(OH)_{7.64}(NO_3)_{0.06}(CO_3)_{0.47}\times 2.4\ H_2O$	64.0 Ni, 9.8 Al, 26.2 O

a turbomolecular pump. Samples had previously been reduced under the same conditions in which the catalyst had been prepared. After reduction, the hydrogen on the nickel surface was removed with 30 mL/min of He for 30 min at 410 °C. The sample was subsequently cooled to 30 °C under the same He stream. The chemisorbed hydrogen was analyzed at 30 °C. The surface of the nickel atoms was calculated assuming a stoichiometry of one hydrogen molecule adsorbed for every two surface nickel atoms and an atomic cross-sectional area of $6.49 \times 10^{-20}\,m^2$ per Ni atom.

2.4. X-ray diffraction (XRD)

Powder X-ray diffraction (XRD) patterns of the catalysts were obtained with a Siemens D5000 diffractometer using nickel-filtered CuKα radiation. Structural evolutions during thermal treatment in air and under a reducing atmosphere were monitored *in situ* with a high-temperature XRD attachment. The patterns were recorded over a range of 2θ angles from 5 to 85°, and compared to the X-ray powder references to confirm phase identities. Particle size for the oxidic and reduced phases was calculated with the Scherrer equation applied to the more intense diffraction lines.

2.5. Thermal analysis

The thermogravimetric (TG) analyses were carried out on a Perkin-Elmer TGA 7 microbalance with an accuracy of 1 μg and equipped with a 0–1000 °C programmable temperature furnace. Samples of 25 mg were heated at 5 °C/min up to 900 °C in a flow of dry helium (80 mL/min). The nature of the gases evolved during the thermal decomposition process was monitored with a QTMD FISONS mass spectrometer.

2.6. Reactor set-up

Experiments were performed in a tubular reactor, which has been described in detail elsewhere [22]. The unit consisted of a catalytic packed-bed reactor, constructed with a 12.7 mm (1/2 in.) o.d. 316-L stainless steel tube, mounted inside an electric furnace. Temperatures in the catalytic bed were measured with three 0.5 mm o.d. thermocouples (type K), placed at different heights inside a 3.18 mm (1/8 in.) o.d. 316-L stainless steel sheath along the center of the reactor. The first thermocouple (TI 02) measured the temperature at the beginning of the bed, the second (TI 03) at half the height of the bed, and the last (TI 04) at the outlet to the bed. For each experiment, the differences in temperature between these three measurements never exceeded 10 °C. The catalytic bed was therefore considered to operate isothermally and the average temperature of the bed was used as the temperature of the catalyst. Water and sunflower oil were pumped at room temperature by two electronic metering pumps and vaporized in preheaters before they entered the reactor. Nitrogen was mixed with steam in the preheater and used as carrier gas and internal standard for gas analysis by gas chromatography. Non-converted fractions were recovered in a system of condensers and cold traps. The catalyst was grounded and sieved to the range 0.20–0.30 mm, and 0.8 g of catalyst was loaded into the reactor. The catalyst was diluted with approximately 12 g of tabular α-alumina T-60 (ALCOA) of the same size so that the endothermic character of the reaction would not produce any excessive gradients in the catalyst bed.

2.7. Product analysis

The gas composition of the product was determined with an on-line HP 5890A gas chromatograph equipped with a Carboxen 1000 packed-bed column (mesh 60/80, 1.5 m long and 3.18 mm (1/8 in.) o.d.), and a thermal conductivity detector. A pneumatic 10-way valve (VALCO A-4C10UWT) was used to inject the sample through a 1 mL sample loop, and helium was used as the reference gas. This configuration allowed hydrogen, nitrogen, methane, carbon dioxide, carbon monoxide, acetylene, ethylene, ethane, and a C_3^+ peak to be separated simultaneously in an analysis that ran for 20 min. The organic phase of the liquid condensed at the reactor outlet was measured and analyzed. The elemental composition was obtained with a Carlo Erba EA1108 analyzer and its main components were determined by GC-MS.

2.8. Vegetable oil

This study used a sample of commercial refined sunflower oil. The elemental composition of the oil was determined with a Carlo Erba EA1108 analyzer. The weight percentages of the oil components were 75.9 ± 0.3 for carbon, 12.1 ± 0.2 for hydrogen, and 12.0 ± 0.4 for oxygen, which corresponds to an average formula of $C_{18}H_{34.4}O_{2.1}$.

3. Results and discussion

The dominant parameters for the steam reforming reaction are the catalyst temperature, the molar steam-to-carbon (S/C) ratio, and the amount of feed processed per unit of catalyst, measured as space velocity. In our work we adjusted the space velocity to values that were high enough for the oil not to be completely converted. The range of catalyst temperature we investigated was from 515 to 615 °C and the S/C ratios were 3, 6, and 9. In these conditions the cracking of the oil was minimized and less than 7% of the fatty acids of the oil were degraded by cracking [22]. Table 2 shows the remaining experimental conditions for the steam reforming of

Table 2
Steam reforming of sunflower oil: operating conditions, product gas flow rate, and gas composition. All experiments were conducted at a sunflower oil flow rate of 0.4 g/min, a carrier gas (N_2) flow rate of 0.26–0.29 L/min, and a catalyst load of 0.8 g + 12 g of α-alumina

Run no.	Catalyst	S/C ratio (mol/mol)	Temperature (°C)		Reactor pressure (bar)	Time on stream (min)	Gas flow rate (L/min) [a]	Gas composition (%)							
			Furnace	Average				H_2	CO	CO_2	CH_4	C_2H_2	C_2H_4	C_2H_6	C_3^+
201	Cat_1	9	650	577	2.83	60	1.80	68.5	4.5	24.2	2.7	0.0	0.0	0.0	0.0
202			600	547	2.67	63	1.20	70.9	2.0	26.0	0.9	0.0	0.1	0.1	0.0
203			550	514	2.53	41	0.62	71.8	0.8	27.0	0.2	0.0	0.1	0.1	0.0
198		6	650	589	2.12	58	2.10	67.9	5.1	24.1	2.7	0.0	0.1	0.1	0.0
199			600	551	2.09	60	1.28	70.0	3.2	25.2	1.5	0.0	0.1	0.1	0.0
200			550	521	1.96	60	0.73	71.4	1.3	26.6	0.4	0.0	0.1	0.1	0.0
233		3	650	610	1.53	60	1.81	65.6	10.0	20.6	3.6	0.0	0.2	0.1	0.0
234			600	580	1.43	60	1.38	68.1	5.6	23.5	2.6	0.0	0.1	0.1	0.0
206			550	536	1.24	60	0.55	70.4	2.2	26.2	0.9	0.1	0.1	0.1	0.0
217	Cat_2	9	650	587	2.22	60	1.46	69.5	4.2	24.3	1.7	0.0	0.1	0.0	0.0
180			600	553	1.49	100	0.93	71.7	2.0	25.7	0.4	0.0	0.1	0.1	0.0
218			600	552	2.11	60	0.91	71.3	1.9	26.0	0.6	0.0	0.1	0.0	0.0
181			550	516	1.39	100	0.46	72.1	0.8	26.8	0.1	0.0	0.1	0.1	0.0
219			550	515	1.95	60	0.50	71.8	0.7	27.1	0.2	0.0	0.1	0.0	0.0
214		6	650	589	1.67	60	1.56	67.5	6.4	23.1	2.8	0.0	0.1	0.0	0.0
215			600	556	1.60	60	1.05	69.5	3.4	25.1	1.8	0.0	0.1	0.1	0.0
216			550	524	1.47	60	0.60	71.3	1.4	26.7	0.4	0.0	0.1	0.0	0.0
220		3	650	606	1.22	60	1.42	66.6	9.0	21.1	3.0	0.0	0.2	0.1	0.0
221			600	571	1.04	60	0.94	68.9	4.6	24.2	1.7	0.3	0.2	0.1	0.0
222			550	535	0.82	60	0.51	70.8	2.0	26.2	0.7	0.1	0.2	0.1	0.0
192	Cat_3	9	650	597	1.78	62	1.32	70.7	3.8	24.3	0.9	0.0	0.2	0.1	0.0
193			600	558	1.67	61	0.79	71.2	1.9	26.1	0.5	0.1	0.2	0.1	0.0
194			550	519	1.57	60	0.41	72.3	0.8	26.5	0.2	0.0	0.1	0.1	0.0
189		6	650	600	1.32	60	1.47	69.0	5.8	23.3	1.6	0.1	0.1	0.1	0.0
190			600	564	1.25	60	0.97	71.0	2.9	25.0	0.8	0.1	0.1	0.1	0.0
191			550	528	1.14	60	0.54	71.9	1.3	26.3	0.3	0.0	0.1	0.1	0.0
195		3	650	613	0.78	60	1.07	66.0	10.6	19.7	3.0	0.2	0.3	0.3	0.0
196			600	580	0.74	66	0.71	68.2	5.7	23.2	2.3	0.1	0.3	0.2	0.0
197			550	539	0.66	60	0.39	71.2	1.9	25.7	0.7	0.1	0.2	0.1	0.0

[a] N_2-free basis.

sunflower oil with our catalysts and the gas flow rate and gas composition for each experiment. The activity of the catalysts was monitored by the extent of oil conversion and by the production of hydrogen, which was measured in moles of hydrogen produced per mass of catalyst (in g) and time (in h). Oil conversion was calculated from the amount of carbon contained in the oil feed and the amount converted to carbon-containing gases by the steam reforming reactions (CO, CO_2, and CH_4). The results for oil conversion and hydrogen production are shown in figures 1 and 2, respectively, for the three catalysts. As a general trend, higher temperatures increased the reaction rate and more carbon from the feed was converted to gas products (CO_2, CO, CH_4, C_2, and C_3^+); C_2 and C_3^+ were formed exclusively through cracking [22] and were always present in very minor amounts (<2% of feed). Depending on the combination of catalyst and operating conditions, between 18 and 97% of the carbon contained in the oil was converted to reforming products (CO_2, CO, CH_4). The concentration of hydrogen in the gas was around 70% for all the experiments, even for different catalysts, reaction temperatures, and S/C ratios, while the concentrations of CO_2, CO, and CH_4 were strongly dependent on the reaction conditions.

From highest to lowest the activity of the catalysts was Cat_1 > Cat_2 > Cat_3, regardless of the reaction temperature and the steam-to-carbon ratio. Oil conversion (figure 1) for the first catalyst (Cat_1) was similar at S/C ratios of 6 and 9, but it was significantly lower at an S/C ratio of 3. For instance, at a reforming temperature of 580 °C oil conversion was 0.53 at an S/C ratio of 3, but around 0.95 at an S/C of 6 and 9. The activity of the second catalyst (Cat_2) was lower than that of Cat_1 at all the combinations of temperature and S/C ratio we tested. It was also less active at an S/C of 3 and the oil conversion at an S/C of 6 was consistently higher than at an S/C of 9; at 590 °C oil conversion was 0.79 and 0.71 for S/C ratios of 6 and 9, respectively. Finally, Cat_3 was the least active of the three and its qualitative behavior was equivalent to that of Cat_2: its lowest activity was at an S/C ratio of 3 and the highest at 6. Trends were similar

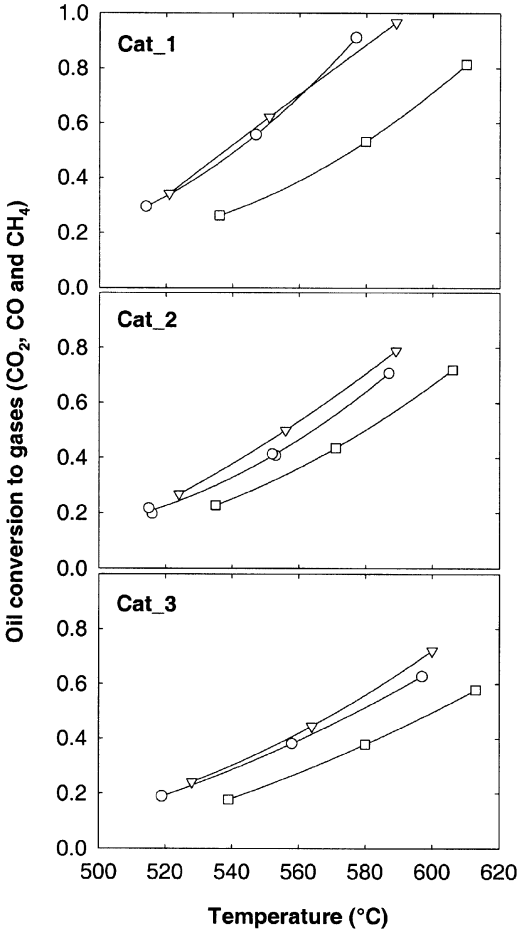

Figure 1. Oil conversion to gas products as a function of reforming temperature for the three catalysts. Steam-to-carbon ratios: 3 (□), 6 (▽), and 9 (○). Lines only indicate trends.

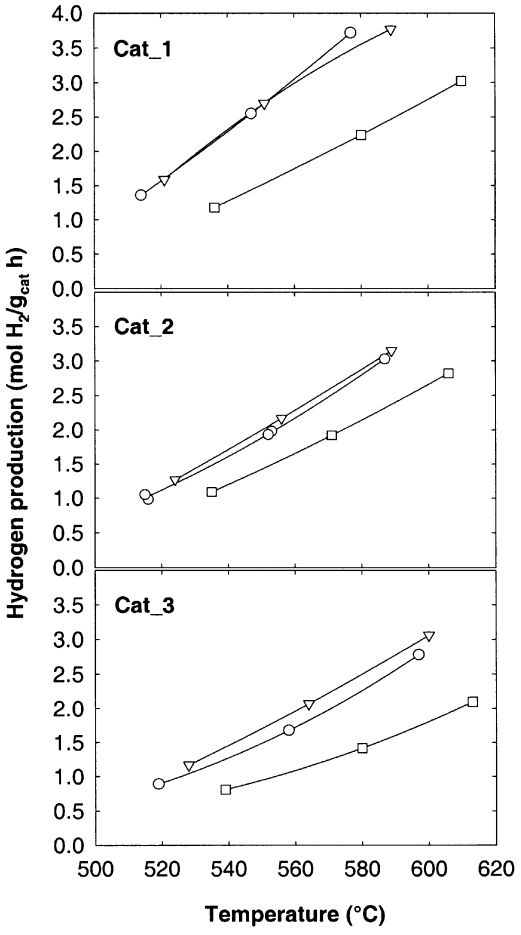

Figure 2. Hydrogen production as a function of reforming temperature for the three catalysts. Steam-to-carbon ratios: 3 (□), 6 (▽), and 9 (○). Lines only indicate trends.

when the production of hydrogen was analyzed (figure 2). For instance, at a catalyst temperature of 550 °C and an S/C ratio of 6, hydrogen production values were 2.7, 1.9, and 1.6 mol $H_2/(g_{cat}\,h)$ for Cat_1, Cat_2, and Cat_3, respectively. Moreover, Cat_1 had similar hydrogen productions at S/C ratios of 9 and 6, but the reaction rate decreased when the S/C ratio was lowered to 3. Cat_2 and Cat_3 had better hydrogen productions at an S/C ratio of 6 than at an S/C ratio of 9. The different behaviors of the catalysts must be due to their surface characteristics and the mechanism of the steam reforming reaction.

It is commonly accepted that the mechanism of the steam reforming process involves the organic molecule being adsorbed onto the metal surface of the catalysts (nickel), where it reacts with water molecules that are adsorbed onto the alumina that supports the metal particles (reaction 1). The primary reaction products are hydrogen and carbon monoxide, which subsequently react to form carbon dioxide and methane through the water-shift (reaction 2) and the methanation (reaction 3) equilibrium reactions [40–44]. The adsorption of the organic molecule onto the metal sites appears to be the limiting step of the reaction process, and water molecules can also be adsorbed onto the metal surface and even react with the organic adsorbed from the gas phase.

$$C_nH_mO_k + (n-k)H_2O \rightarrow nCO + (n + m/2 - k)H_2 \quad (1)$$

$$CO + H_2O \rightleftharpoons CO_2 + H_2 \quad (2)$$

$$CO + 3H_2 \rightleftharpoons CH_4 + H_2O \quad (3)$$

$$C_nH_mO_k + (2n-k)H_2O \rightarrow nCO_2 + (2n + m/2 - k)H_2 \quad (4)$$

The overall steam reforming reaction of an organic compound ($C_nH_mO_k$) is the combination of reactions (1) and (2) and can be expressed according to reaction (4), which gives the maximum hydrogen yield that can be obtained stoichiometrically. Temperature did not substantially affect the hydrogen mole fraction at equilibrium in the range that we studied, but it had a significant effect on the distribution of carbon among CO, CO_2, and CH_4, as we have observed experimentally. Higher temperatures tend to decrease the equilibrium concentrations of methane and carbon dioxide and to increase the concentration of carbon monoxide. In this

Table 3
Characteristics of the Ni-based catalysts obtained by calcination of the hydrotalcite-like precursors at 673 K and reduction at 873 K

Catalyst	BET area (m^2/g)	Metal area (m^2/g)	XRD phases detected [a]	
			Before reaction	After reaction
Cat_1	130.0	12.8	Ni (5.6)	Ni (21.1), NiO
Cat_2	104.0	17.2	Ni (6.7)	Ni (23.0), NiO
Cat_3	96.0	12.5	Ni (8.4)	Ni (28.2), NiO

[a] Numbers in parentheses are particle sizes (in nm) calculated by the Sherrer equation.

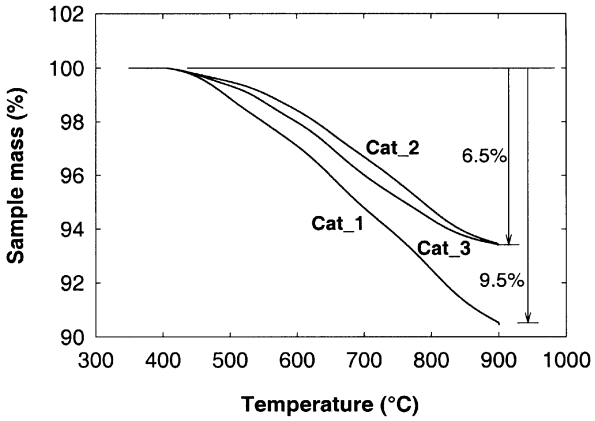

Figure 3. Determination of water adsorbed on the spent catalysts by TGA.

case, the hydrogen released by the disappearance of methane was consumed when CO_2 was transformed into CO, and the hydrogen concentration remained almost constant.

The surface characteristics of the catalysts were analyzed by XRD, BET surface, H_2 chemisorption, and TGA. The values of the BET area, the metal surface, the main phases detected by X-ray diffraction, and the size of the nickel particles, before and after the reaction, are reported in table 3. The most active catalyst, Cat_1, had a metal area of 12.8 m^2/g, while Cat_2 had 17.2 m^2/g and Cat_3 12.5 m^2/g. Although Cat_3 had the highest nickel content it had the lowest metal area, because of the lower dispersion of the metal. The diameter of the nickel particles was found to be approximately 8.4 nm for this catalyst, while it was 5.6 and 6.7 nm for Cat_1 and Cat_2, respectively. The activity of Cat_3 was lower than that of Cat_1 and Cat_2 and this is consistent with the low metal area and nickel dispersion. However, the metal area by itself does not explain why the activity of Cat_1 (12.8 m^2/g) is considerably higher than that of Cat_2 (17.2 m^2/g). When the values of the BET areas are considered it is observed that this parameter increases together with the catalyst activity. Cat_1 has a BET area of 130 m^2/g, while those of Cat_2 and Cat_3 are 104 and 96 m^2/g, respectively. As expected, the BET area of the catalyst increased as the aluminum content rose and the amount of nickel was lower. This trend is consistent with the reaction mechanism: the higher the BET area is, the more water is adsorbed on the catalyst surface, which can react with the organic molecules adsorbed on the metal active sites, and the reaction proceeds faster. The capacity for water adsorption was measured by TGA in an inert atmosphere on samples of the catalyst used. The samples were held at 300 °C for 1 h before the analysis to eliminate moisture, in such a way that only the water molecules that were chemisorbed were kept in the sample. Figure 3 shows the total weight loss as the temperature was increased from 400 to 900 °C at a heating rate of 10 °C/min. Cat_1 had a weight reduction of 9.5%, while Cat_2 and Cat_3 had values of 6.5%. These results are in agreement with their BET areas (130 m^2/g for Cat_1, 104 m^2/g for Cat_2, and 96 m^2/g for Cat_3).

Considering the previous results and the reaction mechanism of steam reforming, we can explain qualitatively the behavior of the catalysts we prepared from hydrotalcite-like materials. The organic molecules (fatty acids) were adsorbed on the metal sites, while the steam molecules were preferentially adsorbed on alumina. The optimum situation was when steam was adsorbed on the support and reacted in the metal interface with the organic that adsorbed there, but as the partial pressure of steam increased water molecules competed with the organic molecules for the metal sites. For Cat_1, increasing the S/C ratio from 3 to 6 caused a significant increase in conversion and hydrogen production, but further increasing the S/C ratio to 9 did not have a significant effect. The situation was the same for Cat_2 and Cat_3 when the S/C ratio was increased from 3 to 6, but when the S/C ratio was increased from 6 to 9 for both catalysts the conversion and hydrogen production decreased. This was due to the fact that steam competed for the metal surface at high partial pressures of steam. This was not so important for Cat_1 because of its greater capacity for water adsorption. The capacity for water adsorption also explains why Cat_1 was more active than Cat_2 despite its lower metal area. At an S/C ratio of 3 the H_2 production for these catalysts is only slightly different, but at higher S/C ratios Cat_1 became more active than Cat_2. This is because the surface area of Cat_1 was greater and it was capable of accommodating a higher partial pressure of water without the adsorption of the organic molecules onto the nickel particles being affected.

Variations in the catalyst activity were investigated in experiments conducted for a few hours under constant reaction conditions. For instance, figure 4 shows the gas flow rate and the gas composition for a 12 h reforming experiment conducted with Cat_1 at 575 °C, an S/C ratio of 2.9, and an average oil conversion of 0.5. A slight loss of activity was observed after 6 h of reaction, with a minor decrease in the flow rate of product gas.

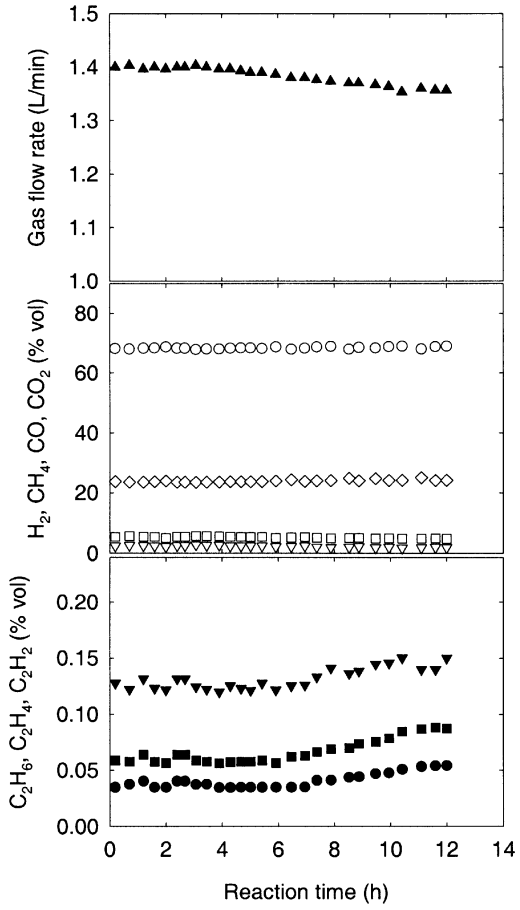

Figure 4. Catalyst activity as a function of reaction time for Cat_1 at a reforming temperature of 575 °C and an S/C ratio of 2.9. Top: gas flow rate (▲). Middle: gas composition, H_2 (○), CH_4 (▽), CO (□), and CO_2 (◇). Bottom: gas composition, C_2H_6 (■), C_2H_4 (▼), and C_2H_2 (●).

There was no significant change in the concentration of the major components of the gas (hydrogen, carbon oxides, and methane), although the concentration of cracking gases (ethane, ethylene, and acetylene) increased somewhat. Similar trends were observed for Cat_2 and Cat_3. The catalysts were characterized after the 12 h reaction period by XRD, and the results are compared with those of the fresh catalysts in figure 5. In the fresh catalysts only the Ni phases were detected in all cases. Although a NiO phase may also be present, it was not detected because it did not have the degree of crystallinity required for detection. The dispersion of the metal was too high. The samples of catalysts used showed Ni and NiO phases. The NiO phase may appear because of an increase in the amount of NiO produced by the oxidation of the Ni phase, or by an increase in the degree of crystallinity of the NiO due to the high reaction temperature. Sintering of the catalysts was shown to have taken place by calculating the Ni crystal sizes, which increased from 5.6 to 21.1 for Cat_1, from 6.7 to 23.0 for Cat_2, and from 8.4 to 28.2 for Cat_3.

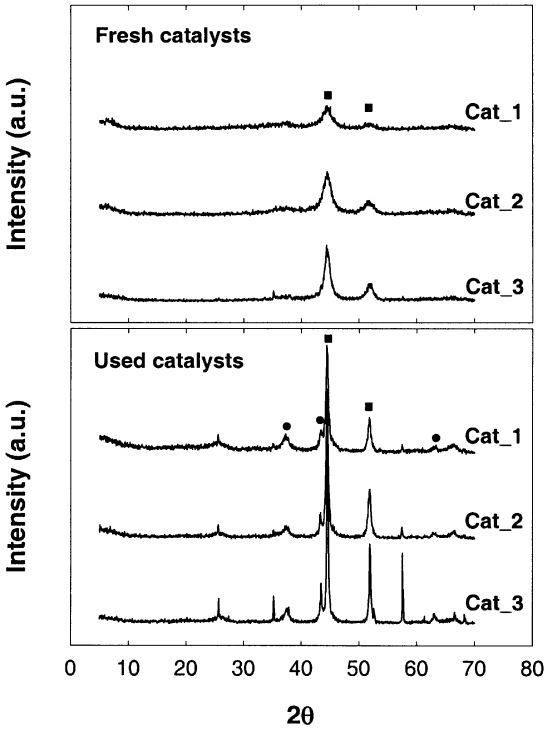

Figure 5. X-ray diffraction spectra of the catalysts before (top) and after reaction (bottom). Main phases detected: ■, Ni; ●, NiO.

4. Conclusions

Three hydrotalcite-like materials with different Ni/Al atomic ratios were synthesized and used to prepare steam reforming catalysts. The catalysts were characterized by XRD, BET areas, TGA, and hydrogen chemisorption techniques. After the hydrotalcites had been calcined, well-dispersed NiO particles were obtained. Their crystallite sizes decreased when the nickel content was lower. The reduction of the NiO phase also depended on the nickel content. Low nickel content gave rise to lower reduction degrees and higher BET areas.

The catalysts were tested for the steam reforming of sunflower oil to produce hydrogen, and it was shown that the catalyst with the lowest nickel content (Cat_1) had the highest activity throughout the range of temperatures and S/C ratios we covered. This is because of its smaller nickel crystallite size and higher BET area and water adsorption capacity. The catalysts showed some sintering after 12 h of reaction, although much longer experiments are required if the extent of catalyst sintering and deactivation is to be assessed.

Acknowledgments

The authors are indebted to the Spanish Government (MCYT, project PPQ2001-1215-CO3-01) and to the Catalan Regional Government (CIRIT, project 2000SGR-00104) for financial support.

References

[1] J. Quakernaat, Int. J. Hydrogen Energy 20 (1995) 485.
[2] J.N. Armor, Appl. Catal. A: Gen. 176 (1999) 159.
[3] D.E. Ridler and M.V. Twigg, in: *Catalysis Handbook*, ed. M.V. Twigg (Wolfe Publishing, Cleveland, UK, 1989).
[4] P.L. Spath and M.K. Mann, National Renewable Energy Laboratory (NREL), Golden, CO, TP-570-27637 (2000).
[5] B. Gaudernack and S. Lynum, Int. J. Hydrogen Energy 23 (1998) 1087.
[6] T.A. Milne, C.C. Elam and R.J. Evans, Report for the International Energy Agency Agreement on the Production and Utilization of Hydrogen, IEA/H_2/TR-02/001 (2001).
[7] R.J. Evans, R.A. Knight, M. Onischak and S.P. Babu, in: *Proceedings of Energy from Biomass and Wastes X*, ed. D.L. Klass (Institute of Gas Technology, Chicago, IL, 1988).
[8] W.B. Hauserman, Int. J. Hydrogen Energy 19 (1994) 413.
[9] L. García, M.L. Salvador, J. Arauzo and R. Bilbao, Energy Fuels 13 (1999) 851.
[10] M. Caballero, J. Corella, M. Aznar and J. Gil, Ind. Eng. Chem. Res. 39 (2000) 1143.
[11] E. Chornet, D. Wang, D. Montané, S. Czernik, D. Johnson and M. Mann, in: *Proceedings of the 1995 U.S. DOE Hydrogen Program Review*, NREL/CP-430-20036 (National Renewable Energy Laboratory, Golden, CO, 1995), p. 707.
[12] M. Mann, P. Spath and K. Kadam, in: *Proceedings of the 1995 U.S. DOE Hydrogen Program Review*, NREL/CP-430-20036 (National Renewable Energy Laboratory, Golden, CO, 1995), p. 205.
[13] D. Wang, D. Montané and E. Chornet, Appl. Cat. A: Gen. 143 (1996) 245.
[14] D. Wang, S. Czernik, D. Montané, M. Mann and E. Chornet, Ind. Eng. Chem. Res. 36 (1997) 1507.
[15] D. Wang, S. Czernik and E. Chornet, Energy Fuels 12 (1998) 19.
[16] M. Marquevich, S. Czernik, E. Chornet and D. Montané, Energy Fuels 13 (1999) 1160.
[17] S. Caballaro and S. Freni, Int. J. Hydrogen Energy 21 (1996) 465.
[18] S. Freni, G. Maggio and S. Caballaro, J. Power Sources 62 (1996) 67.
[19] F.J. Mariño, E.G. Cerrella, S. Duhalde, M. Jobbagy and M.A. Laborde, Int. J. Hydrogen Energy 23 (1998) 1095.
[20] M. Marquevich, R. Coll and D. Montané, Ind. Eng. Chem. Res. 39 (2000) 2140.
[21] M. Marquevich, F. Medina and D. Montané, Catal. Commun. 2 (2001) 119.
[22] M. Marquevich, X. Farriol, F. Medina and D. Montané, Ind. Eng. Chem. Res. 40 (2001) 4757.
[23] Y. Ali and M.A. Hanna, Bioresource Technol. 50 (1994) 153.
[24] M. Stumbort, A. Wong and E. Hogan, Bioresource Technol. 56 (1996) 13.
[25] F. Karaosmanoglu, K.B. Cigizoglu, M. Tüter and S. Ertekin, Energy Fuels 10 (1996) 890.
[26] R. Allmann and H.H. Lohse, N. Jhb. Miner. Mh. 6 (1966) 161.
[27] L. Ingram and H.P. Jepsen, N. Jhb. Miner. Mh. 36 (1967) 465.
[28] H.F.W. Taylor, Miner. Mag. 39 (1973) 377.
[29] Bhattacharyya, V.W. Chang and D.J. Shumacher, Appl. Clay Sci. 13 (1998) 317.
[30] F. Cavani, F. Trifiro and A. Vaccari, Catal. Today 11 (1991) 173.
[31] D. Tichit, B. Coq, S. Ribet, R. Durand and F. Medina, Stud. Surf. Sci. Catal. 130A (2000) 503.
[32] F. Trifiro and A. Vaccari, Compr. Supramolec. Chem. 7 (1996) 25.
[33] Corma, V. Fornes, R.M. Martin-Aranda and F. Rey, J. Catal. 134 (1992) 58.
[34] F. Medina, D. Tichit, B. Coq, A. Vaccari and N.T. Dung, J. Catal. 167 (1997) 142.
[35] D. Tichit, M.H. Lhouty, A. Guida, B.H. Chiche, F. Figueras, A. Auroux, B. Bartalini and E. Garrone, J. Catal. 151 (1995) 150.
[36] P. Courty, D. Durand, E. Freund and A. Surgier, J. Mol. Catal. 17 (1982) 241.
[37] P. Gherardi, O. Ruggeri, F. Trifiro, A. Vaccari, G. Del Piero, G. Manara and B. Notari, Stud. Surf. Sci. Catal. 16 (1983) 723.
[38] E.C. Druissink, L.L. Van Reijen and J.R.H. Ross, J. Chem. Soc., Faraday Trans. I 77 (1981) 649.
[39] H.G.J. Lansink Rotgerink, H. Bosch, J.G. Van Ommen and J.R.H. Ross, Appl. Catal. 27 (1986) 41.
[40] G.W. Bridger and W. Wyrwas, Chem. Proc. Eng. Sept. (1967) 101.
[41] C.R. Schnell, J. Chem. Soc. B (1970) 158.
[42] J.R. Rostrup-Nielsen, Chem. Eng. Prog. 73 (1977) 87.
[43] J. Xu and G.F. Froment, AIChE J. 35 (1989) 88.
[44] P.A. Simell, E.K. Hirvensato, V.T Smolander and A.O.I. Krause, Ind. Eng. Chem. Res. 38 (1999) 1250.